3

Evaluation of Solar Spectra and Their Effects on Radiative Transfer and Climate Simulation

Zhian Sun[1], Jiangnan Li[2] and Jingmiao Liu[3]
[1]*Centre for Australian Weather and Climate Research, Australian Bureau of Meteorology*
[2]*Canadian Centre for Climate Modelling and Analysis, Science and Technology Branch, Environment Canada, University of Victoria*
[3]*Chinese Academy of Meteorological Sciences*
[1]*Australia*
[2]*Canada*
[3]*China*

1. Introduction

In this chapter we will discuss solar spectral distributions and their corresponding impact on the climate, especially on the Earth's atmospheric temperature and energy balance at the surface. Solar spectrum is defined as a spectral distribution of the solar radiation at the top of the atmosphere (TOA). It represents the incoming solar energy to the earth system containing the atmosphere and ocean. Solar radiation is the original driving force for the continuous circulations of atmosphere and ocean. It has been recognized that the variation of total solar irradiance (solar constant) at the TOA is one of the important factors impacting climate change, though the variation in total solar irradiance is very small, approximately only about 0.1% of the solar constant or about 1.3 W m^{-2} (Krivova *et al*, 2010). Besides the variation of the total solar irradiance the changes in the spectral distribution of the solar radiation can also affect the climate. However much less attention has been focused on this aspect.

The solar radiation at different wavelengths penetrates Earth's atmosphere to different depths. The high energy ultraviolet (UV) radiation is mostly absorbed by ozone in the mesosphere and stratosphere. The atmosphere is relatively transparent to the visible (VIS) radiation and allows most visible radiation to reach the earth's surface and heat the land and ocean surfaces. The atmosphere has strong absorption in the near infrared (NIR) radiation mainly due to the water vapor in the lower troposphere. Therefore, different solar spectral distributions at the TOA can affect the temperature structure in the atmosphere and the energy balance at the surface, and hence impact the weather and climate.

In this chapter, the most commonly used solar spectra will be summarized and their characteristics compared. These solar spectra will be applied to off-line radiation calculations and climate model simulations to quantify the impact on climate.

2. Measurement of the solar spectrum

Since the 1970s, the measurement of the solar spectral distribution at the TOA has become an important issue for climate modeling. Since then several solar spectra have been proposed and widely used. The solar spectrum can be measured at the earth's surface and on space platforms or estimated using proxy indicators such as sunspot and faculae. Before satellite measurements of the solar spectrum became available, the data were mainly from ground-based measurements and laboratory experiments. Since the historical time series of the solar spectrum is required for long-term climate simulations and the data from observations are not long enough for this purpose, reconstruction of the solar spectral time series using empirical regression is inevitable. The most commonly used solar spectrum in the early period was that provided by Neckel and Labs (1984) which was derived from long-term observations of the absolute solar intensity measured at Kitt Peak Observatory and from aircraft measurements. This solar spectrum became the reference and was used by many science communities such as radiation model groups and the remote sensing community. We refer to this solar spectrum as Neckel-Labs in the following discussions.

The second solar spectrum commonly used in the scientific community is that developed by Kurucz (1995) based on measurements at Kitt Peak Observatory and balloon-based measurements. This is a synthetic solar spectrum derived by a combination of measurements and a theoretical model. The development of this spectrum was motivated by research work performed by Gao and Green (1995) who found that the standard spectrum from Neckel-Labs contains many absorption features in the 2.0-2.5 μm region that cannot be seen in the observations from shuttle-borne instruments. These absorption features have been corrected in the refined Kurucz spectrum. We refer to this solar spectrum as Kurucz95. The advantage of the Kurucz95 spectrum is its high spectral resolution ($\sim$1 cm^{-1}) which is required by certain research applications, such as offline studies with line-by-line radiative transfer models. Since this spectrum was published it has been used by several organizations such as the UK Met Office, the US Atmospheric Environment Research and the Australian Bureau of Meteorology, etc,. The Kurucz95 spectrum was recently updated by Chance and Kurucz (2010) who corrected the absorption of solar irradiance by ozone and imported the cross-calibration with the solar spectrum measured from satellite. We refer to this updated version as Kurucz10 .

Lean (2000) provided the third solar spectrum which is a reconstruction of spectral irradiance using multi-component empirical models, based on activity indices such as sunspot and facular time series. This spectrum was updated with measurements from satellites from 1983 to 2004 covering the last two solar cycles and has been implemented into the UK Met Office atmospheric model (Zhong *et al.*, 2008). We refer to this spectrum as Lean00.

Satellites make it possible to directly measure the solar spectrum without the confounding influence of the Earth's atmosphere. In recent decades, a number of experiments have been performed on various space platforms which have resulted in the new and improved solar spectrum published by Thuillier *et al*. (2003). The spectrum provided by Thuillier were derived from two instruments flown on the European Retrieval Carrier missions. This spectrum covers the spectral range from 200 nm to 2400 nm and has been cross compared with observations from other missions (Thuillier *et al*., 2003). We combine this data with that

of the Kurucz10 for the wavelengths beyond 2400 nm to form a full spectrum. We use this solar spectrum as the standard reference spectrum.

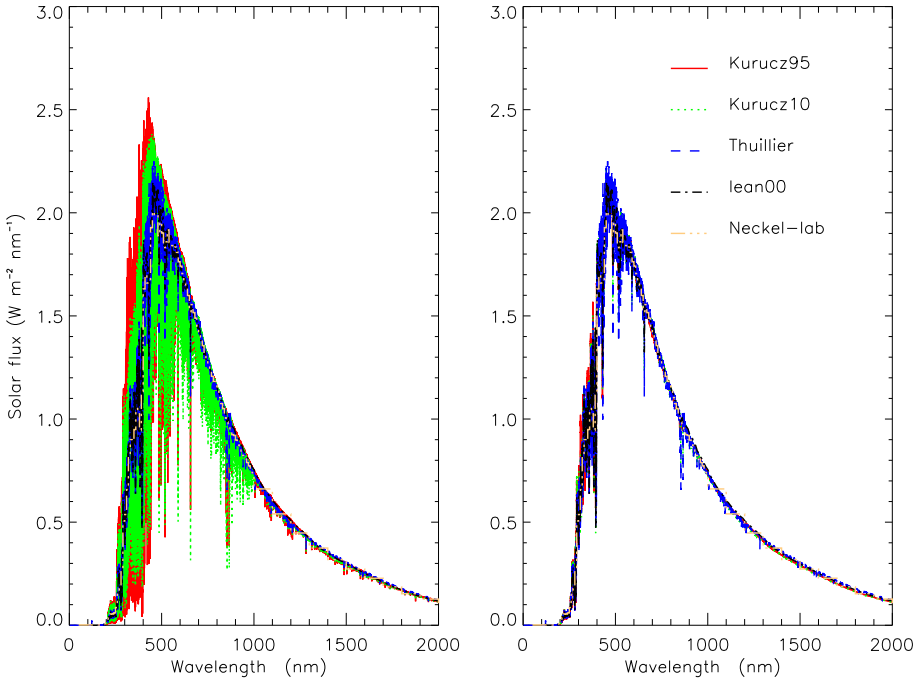

Fig. 1. Spectral distributions of solar irradiance at the top of the atmosphere. Left: plots on the original spectral grids; Right: two Kurucz spectra degraded by a moving average over 0.5 nm.

The five solar spectra mentioned above are shown in Fig.1. The major difference between these spectra is the spectral resolution. The spectral resolutions for the two Kurucz spectra are much higher than for the other three spectra and exhibit large oscillations in the spectral region 200-1000 nm. The right panel shows the two Kurucz spectra degraded by taking a moving average over the 0.5 nm spectral grids of the original spectrum. The degraded curves are relatively smooth and agree better with the other spectra. Chance and Kurucz (2010) also compared their modified spectrum with Thuillier's spectrum using a similar degradation.

It is seen that the spectral distributions of the five solar spectra are different. However, highly oscillatory spectral signatures make it hard to analyze these differences. In order to create a picture that can clearly show the spectral differences between the five solar spectra we calculate the fractional distribution of the incoming solar energy in the three solar spectral ranges of UV, VIS and NIR and the results are shown in Fig.2. The results presented in this figure have been normalized by the reference spectrum of Thuillier to explore the differences relative to the reference spectrum. It is seen that the fractions of the solar energy among the

five spectra are different in these spectral regions. These differences will result in significant differences in the radiative heating rates in the stratosphere and irradiances at the surface as will be shown in the following sections. The roles of the incoming solar energy in these three spectral regions are very different. In the UV region, the ozone absorption is dominant in the mesosphere and stratosphere and most of the solar energy is absorbed here. In the NIR range water vapor is a dominant absorber with the corresponding strong absorption occurring in the lower atmosphere. In the VIS range gaseous absorption is relatively weak allowing a large portion of the solar energy to penetrate through the atmosphere and reach the earth's surface. Therefore, different solar spectral distributions can produce different heating profiles inside the atmosphere and also influence the energy budget at the surface. These physical principles help us to understand the results of the model simulations shown in the following sections.

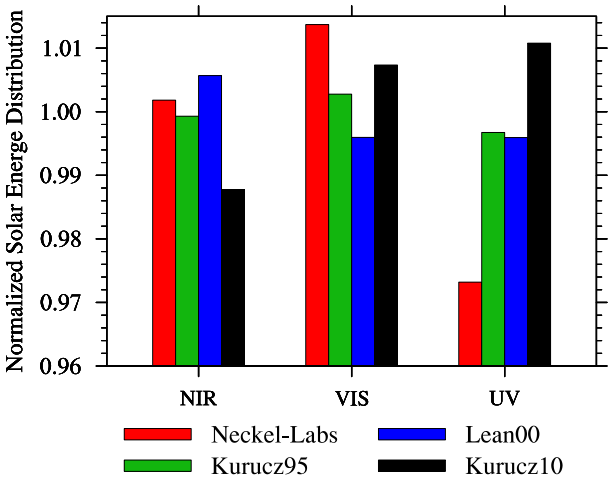

Fig. 2. The fractional distribution of solar energy over three spectral regions from 4 model spectral data. The results have been normalized by the fraction of the Thuillier reference data.

3. Radiation and climate models

In order to study the sensitivity of the different solar spectral distributions, three kinds of model will be used. The first is a high resolution line-by-line model, which is usually used as a benchmark to verify the accuracy of a radiation algorithm used in a climate model, but in this study, we use it to evaluate irradiance at the surface and the heating rate in the atmosphere determined using the different solar spectral data. With the line-by-line calculations, the detailed changes in the heating rates and irradiances corresponding to the variations of the solar spectral distributions can be revealed. The line-by-line radiative transfer model GENLN2 (Edwards, 1992) is used to perform these calculations at high spectral resolution. Version 3.0 of the GENLN2 model is used and this model has been modified to allow irradiance and heating rates calculations.

The broad-band model used in this study is the Sun-Edwards-Slingo version 2 (SES2) scheme (Sun, 2011). It has 9 spectral bands in the shortwave region, 4 bands in the UV-VIS and 5 bands

in the NIR. The 5 solar spectra have been implemented in the scheme so that their impact on radiative heating in the atmosphere can be assessed in both off-line calculations and in climate model simulations.

The Australian Community Climate Earth System Simulator (ACCESS) model is used to perform the climate sensitivity study. ACCESS is a fully coupled system developed at the Centre for Australian Weather and Climate Research. The atmospheric component is the UK Met Office Unified Model. The SES2 radiation has been implemented in ACCESS. We performed AMIP (Atmospheric Model Intercomparison Project) type simulations to assess the impact of the variation of solar spectrum on the earth's climate. The model used in this study has a horizontal resolution of 1.25° x 1.875° in latitude and longitude and 85 vertical levels. The model top height is about 85 km. The model dynamical core is a semi-implicit, semi-Lagrangian, predictor-corrector scheme solving the non-hydrostatic, deep-atmosphere equations (Davies *et al.*, 2005). In addition, the model includes a prognostic cloud fraction and condensate cloud scheme.

4. Impact of solar spectral distribution

There have been a number of studies investigating the possible impact on climate due to changes in the solar constant (e.g. Kopp and Lean, 2011), but there is a lack of systematic research on the intercomparison of those solar spectra mentioned above and the impact on climate model simulations due to the differences in these spectra. Mlawer *et al.* (2000) compared the solar spectral irradiance at the surface determined with their line-by-line model (LBLRTM) using the Neckel-Labs and Kurucz95 spectra with high spectral resolution observations obtained at the Southern Great Plains site of the US Atmospheric Radiation Measurement (ARM) program(Stokes and Schwartz, 1994). Their results suggested that Kurucz95 provides a better modelled irradiance at the surface. Zhong *et al*. (2008) compared the impact of shifting from the Neckel-Labs spectrum to the Kurucz95 and Lean00 spectra in a line-by-line radiation model and in a climate model. They found that the solar heating rate in the stratosphere generated by Kurucz95 is significantly larger than that generated by Neckel-Labs, because the larger incoming solar energy in the UV causes extra ozone absorption in the Kurucz95 spectrum. Since different climate models may use any of the solar spectra introduced above it will be useful to investigate the use of all of the spectra mentioned above and their influence on radiation and climate models, particularly in the context of AMIP style experiments. In addition, the recent satellite observation-based Thuillier spectrum was not accounted for in Zhong *et al*. (2008) and has not been evaluated in climate models. In this section, we present a comparison of the five solar spectral data, in which four of them (Neckel-Labs, Kurucz95, Kurucz10 and Lean00) have been used in AMIP style model simulations. The satellite observation-based Thuillier spectrum is used as the reference. It should be emphasized that although we use the Thuillier spectrum as a reference, it should not be regarded as the standard benchmark because the solar spectrum varies and a spectral data averaged from a longer period may be preferred. An appropriate comparison with observations may be desirable to assess the accuracy of these spectral data but this is beyond the scope of this study.

In Zhong *et al*. (2008), the related physical discussion focused on the temperature bias in the stratosphere due to changing the solar spectra. In our discussions, apart from the stratospheric

temperature issue, more attention is paid to the physics related to the changes in the lower tropospheric temperature and the surface energy balance.

4.1 Off-line radiation calculations

GENLN2 line-by-line calculations are performed using a middle latitude summer (MLS) atmosphere with 107 vertical levels to investigate the impact of the changes in solar spectrum on the solar heating rates in the atmosphere. The HITRAN2008 data base is used and 6 absorbing species (H2O, CO2, O3, CH4, N2O, O2) are included in the calculations. The water vapor continuum and oxygen collision-induced continuum are also included. The spectral resolution of 0.005 cm^{-1} and the Voigt line shape profile are used in the calculations. The solar constant is taken as 1368.8 W m^{-2}, the solar zenith angles is assumed to be 30° and the surface albedo is set to 0.2.

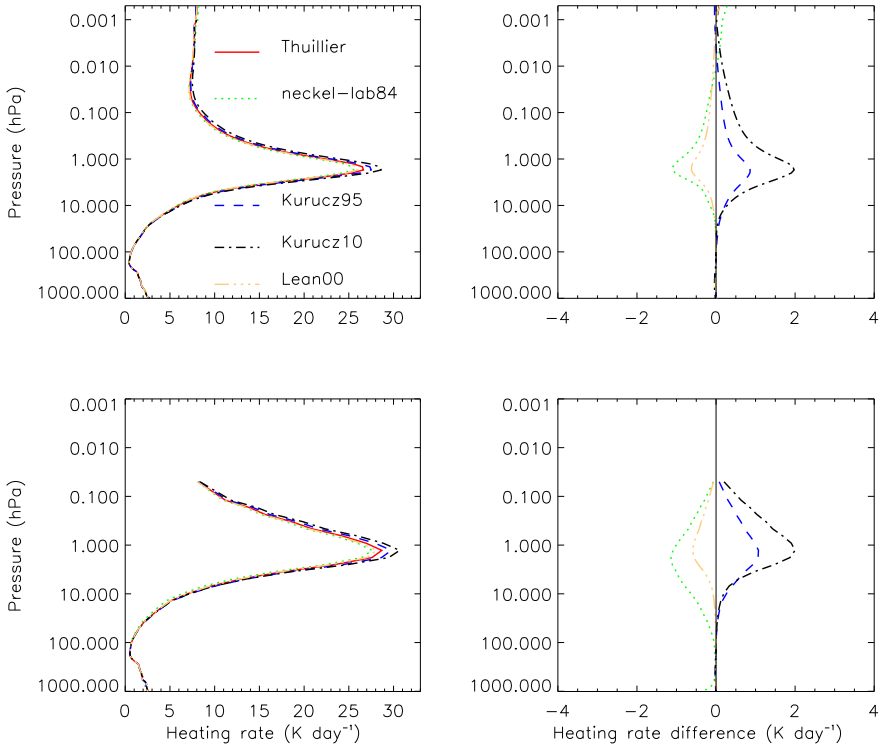

Fig. 3. Solar heating rates determined using GENLN2 line-by-line (upper panels) and SES2 broad-band (lower panels) schemes with five solar spectra. The calculations use the MLS atmosphere with a solar constant of 1368.8 W m^{-2} and a solar zenith angle of 30°. The Thuillier spectrum is treated as the reference and the left panels show the heating difference between the model spectra and this reference.

In Fig. 3, the upper left panel shows the solar heating rates calculated by GENLN2 for the five solar spectra. Taking Thuillier as the reference, the upper right panel shows the differences in heating rate between the model solar spectra and reference spectrum. It is seen that the maximum solar heating rate occurs at about 1 hPa. This is due to the absorption by ozone whose maximum concentration is close to this level. A large difference in heating rate also occurs around this region. Compared to the result from the reference spectrum, it is found that the Neckel-Labs and Lean00 spectra produce smaller heating rates, and the two Kurucz spectra produce larger heating rates. The difference in heating rate between Neckel-Labs and the reference is about -1.5 K day^{-1} and the difference in heating rate between Kurucz10 and the reference is about 2 K day^{-1} , which is about 10% of the heating rate close to 1 hPa. Since the total incoming solar energy is assumed to be the same for all five spectra, in the Neckel-Labs and Lean00 spectra, less solar energy is filtered out by ozone absorption before it reaches the lower atmosphere and ground.

The same calculations are also performed using the SES2 broad-band scheme. In the SES2 model Rayleigh scattering is included. The broad-band calculations use the MLS atmosphere with 60 vertical levels and the rest of the specifications are the same as those for the line-by-line calculations. It can be seen that the results from the broad-band calculations are very close to those of the line-by-line calculations. Since the SES2 radiation algorithm is used in the climate model calculations shown below, the results in 3 indicate that the radiation calculations in the climate model are reliable.

It is seen in Fig.2, the old solar spectrum of Neckel-Labs has the smallest solar energy input in the UV range. This is consistent with the result shown in Fig.3. The heating rate due to ozone absorption is the weakest for Neckel-Labs. It is found that the two Kurucz spectra have relatively large energy fraction in the UV spectral range. Therefore, the solar heating rates from these two spectra are larger than those from the other spectra in the ozone absorption region.

In order to verify the results of Fig.3, in Fig.4 we present the more detailed line-by-line spectral heating rates at the 1.5 hPa level, where the ozone absorption is at its peak value. Only the UV region is shown as the heating rate in other regions is essentially zero. In the upper panel the heating rates from the Kurucz10, Lean and Thuillier calculations are shown as a function of wavelength. It is seen that large heating rates occur in the Hartley band around 300 nm due to the ozone absorption there. Also large differences in heating rate are found in this region using the different solar spectra. The Lean spectrum produces the smallest heating rate and the Kurucz10 spectrum produces the largest heating rate.

Figure 2 shows that the Lean00 spectrum has the largest solar fractional input energy in the NIR region, so it is expected that the use of this spectrum would produce a larger heating rate in the lower troposphere where the water vapor absorption dominates. However, since the air density is high in the lower atmosphere, the heating rate becomes small, and the difference in heating rate is not obviously noticeable in Fig.3. Nevertheless the difference in heating rate in the lower troposphere can be more clearly found in climate simulations as shown later due to feedback effects involving water vapor.

It is also seen in Fig.2, that the two Kurucz spectra and Neckel-Labs spectrum have relatively larger solar input energy in the visible region. Since the atmosphere is relatively transparent

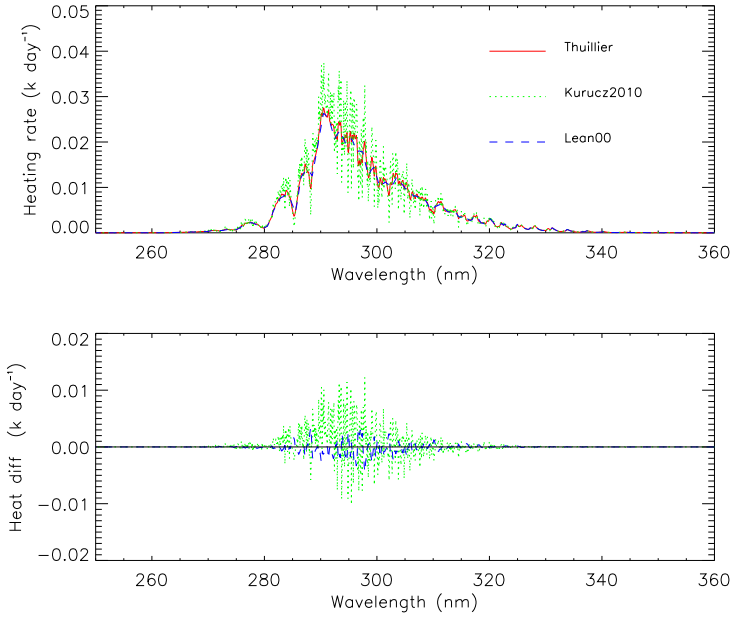

Fig. 4. Solar spectral heating rates at the 1.5 hPa level of a MLS atmosphere determined using the GENLN2 model for three solar spectra. The calculations assume a solar zenith angle of 30° and a surface albedo of 0.2. The lower panel shows the heating differences between Kurucz10, Lean00 and the reference.

in this region, the larger the input solar energy at the TOA will lead to a larger downward solar irradiance at the surface and this is demonstrated in Fig. 5.

In Fig.5, the downward solar irradiances versus solar zenith angle are plotted. The calculations are performed using the GENLN2 model. As in Fig.3, the results are determined taking the spectrum of Thuillier as the reference and the differences in the downward irradiance at the surface between the model spectra and reference are shown. The upper left panel of Fig.5 presents the differences in total downward solar irradiance at the surface. It is found that the downward solar irradiances at the surface obtained using the all four model solar spectra are higher than that using the reference spectrum. The irradiance difference between Kurucz95 and the reference is smallest and the difference between Kurucz10 and the reference is largest. At the solar zenith angle of zero, the Kurucz10 spectrum produces an extra 2 W m^{-2} solar downward irradiance at the surface compared with the result from the reference spectrum.

In order to understand the reason for the difference in the downward flux at the surface, we separate the broad band results into three spectral ranges and the corresponding results are shown in the other three panels. In the UV range (upper right panel), the downward irradiance at the surface from the Kurucz10 spectrum is higher than that from the reference spectrum, while the results from the other three spectra are less than that from the reference. It

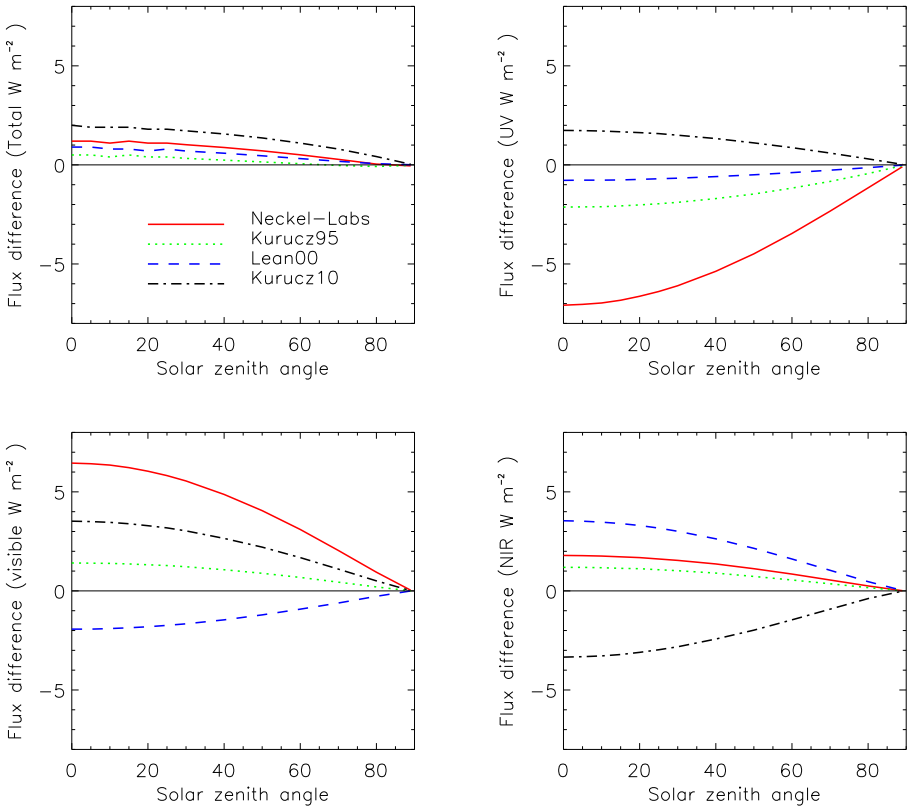

Fig. 5. Difference of downward solar irradiance between model spectra and the reference determined using the GENLN2 model. The upper left panel shows the difference in full spectrum, upper right for the UV spectrum, lower left for the VIS spectrum and lower right for the NIR spectrum.

is shown in Figs.2 and 3 that Kurucz10 has a larger portion of the solar energy in the UV region and produces the largest solar heating rate in the stratosphere. The downward irradiance at the surface is also high using this spectrum. The proportion of the solar energy for the Neckel-Labs spectrum is significantly smaller in this region and the surface irradiance from this spectrum is also small compared with the reference results. The difference in irradiance between Neckel-Labs and the reference can be as large as 7 W m^{-2} at zero solar zenith angle.

The differences in the downward solar irradiance in the VIS range are shown in the lower left panel of Fig.5. Since the atmosphere in the VIS region is relatively transparent to downward solar radiation, the results of the downward irradiance at the surface match well with those of the incoming solar energy at the TOA as shown in Fig.2. The spectrum of Neckel-Labs, Kurucz95 and Kurucz10 have a relatively larger proportion of the solar energy in this region compared with reference spectrum. The downward irradiances at the surface from these three

spectra are higher than that of reference, whereas the downward irradiance from Lean00 is less than the reference due to its relatively less incoming solar energy at the TOA. The difference between Neckel-Labs and Thuillier is close to 7 W m^{-2}, and difference between Neckel-Labs and Lean is up to 9 W m^{-2}.

The differences in downward solar irradiance in the NIR region are shown in the lower right panel of Fig.5. In contrast to the result of the UV, Kurucz10 is the smallest and Lean00 is the largest. According to Fig.2, Kurucz10 contains the smallest proportion of the solar energy compared to the other data, which leads to less downward flux at the surface. Also it is easy to understand why the Lean spectrum has the largest downward irradiance, since the solar incoming energy portion from this data is the largest one amongst the five spectra in the NIR range.

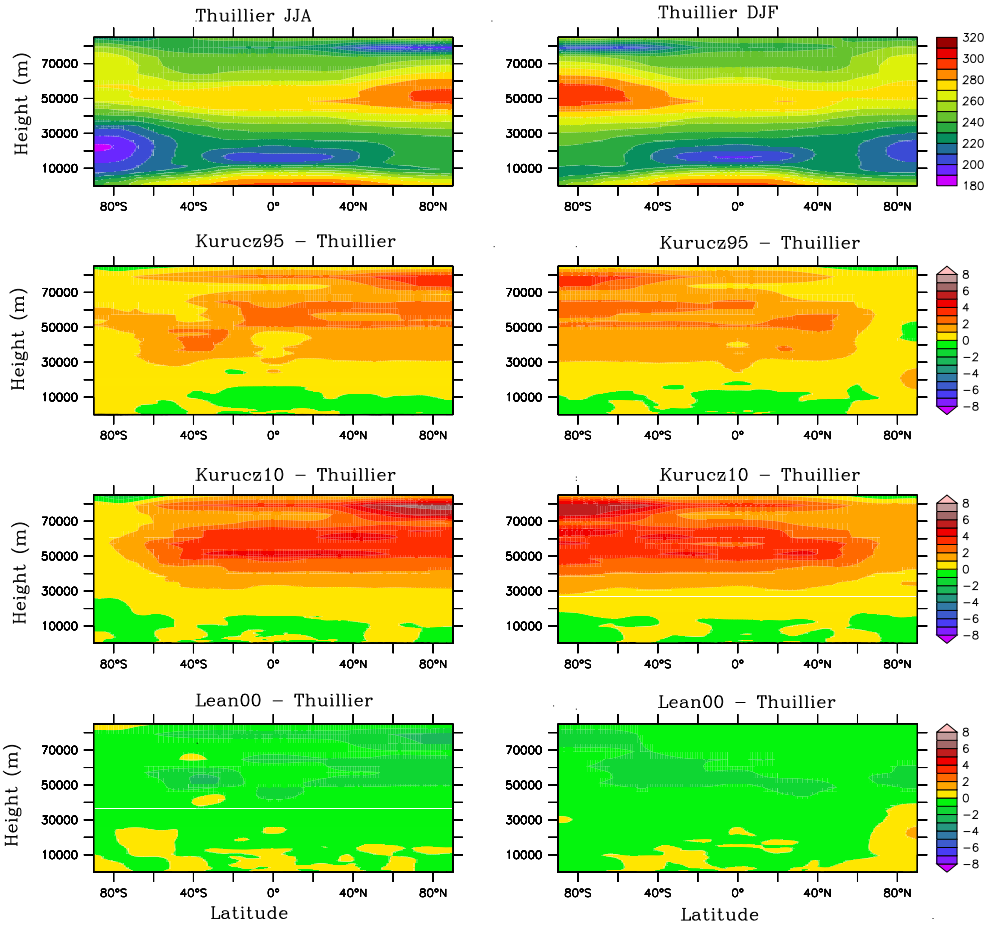

Fig. 6. Zonal mean temperature cross-sections determined by the ACCESS model for two seasons. The upper panels show the results corresponding to the reference solar spectrum and the following panels are the differences due to the model spectra relative to the reference.

Overall the spectral distributions of the downward irradiance at the surface are largely controlled by the distributions of the incoming solar radiation at the TOA, although gaseous absorption in the atmosphere can also have an effect. It is seen that although the changes in the downward total irradiance at the surface are within 2 W m^{-2} corresponding to the changes in spectral distribution at the TOA, the changes in spectral band irradiance are much larger, which will have large impacts on boundary layer and on land-surface processes. In the UV spectral region, for example, the changes in irradiance at the surface will affect the UVB forecasts that are important to the public. Radiation in the visible region (photosynthetically active radiation) is partially absorbed by plants and affects crop production and the carbon balance in the biosphere. In the NIR spectral region, water vapour absorption in the lower troposphere generates significant greenhouse warming. The radiation reaching the surface will be largely absorbed by the land surface because of the small albedo, which will lead to an increase in the surface temperature. The downward solar irradiance at the surface can strongly influence the surface energy budget and the surface sensible and latent fluxes. Therefore seeking an accurate solar spectrum is clearly an important issue for numerical modelling of weather and climate.

4.2 AGCM simulations

In this section, we focus on the impacts of the changes in solar spectral distribution on present-day model-simulated climate. The climate simulations are performed with the ACCESS atmospheric model, which has been discussed in the previous section. The AGCM simulations have been performed with an initial condition specified at September 1978. Prescribed sea surface temperature and sea ice data with seasonal variations are used as forcing from the ocean. A series of 30-year climate integrations were performed in order to find the influence of the different solar spectral distributions on climate simulations. A long time climate model simulation is required to reduce the noise due to natural variability. We present below the 30 year mean climatology.

The climate simulations based on four solar spectra (Thuillier, Kurucz95, Kurucz10 and Lean00) are performed. The Neckel-Labs spectrum is not considered in the climate simulations, since this old solar spectrum has became less popular in the last decade. As for the off-line radiative transfer comparisons, the climate simulation results are based on taking the Thuillier spectrum as the reference. Two seasonal mean results for summer June-July-August (JJA) and winter December-January-February (DJF) are presented.

We first investigate the temperature response inside the atmosphere. Figure 6 shows the zonal mean temperature cross-section for the two seasons and difference between the simulations using the different model spectra and reference spectrum. It is found that higher temperatures occur in the upper stratosphere due to the ozone absorption in the UV region. In the lower atmosphere below 2 km, the temperature is relatively large too due to water vapor absorption in the NIR range. In climate simulations feedback processes can play an important role. The absorption of solar energy in the NIR spectrum can cause a warming effect, and the temperature increase in the atmosphere can lead to more water vapor in return. This kind of feedback can make the temperature bias more sensitive to changes in the incoming solar spectral distribution.

The differences in temperature between the climate simulations using different solar spectra are shown in the lower panels. It is seen that the temperatures in the upper atmosphere from the simulations using the Kurucz95 and Kurucz10 spectra are systematically higher than that using the Thuillier spectrum. The difference can be as large as 5 K over large regions in the upper stratosphere. This is consistent with the results from the off-line line-by-line and broad-band calculations as shown in Figs.3 and 4. In contrast, the temperatures obtained by using the Lean spectrum are systematically lower than that using the Thuillier spectrum. Zhong et al. (2008) have performed GCM simulations to test the effect of the Kurucz95 and Lean solar spectra used in an early version of the UM model. They have shown that the use of the Kurucz95 spectrum results in a substantial warm bias above the stratosphere, and using the Lean spectrum can reduce the warm bias by about 4.3 K. The results obtained here are consistent with their finding. Furthermore, our results indicate that the use of Kurucz10 spectrum can cause an even larger warm bias in the stratosphere, which has not been studied by anyone before.

In the lower atmosphere, the Lean00 spectrum produces a noticeable warming bias compared to that of the Kurucz spectrum. As is shown in Fig.2 the Lean00 spectrum contains a larger portion of the incoming solar energy in the NIR region, and this energy can penetrate through the upper atmosphere and reach the lower troposphere where the water vapor absorption is relatively strong and leading to the larger solar heating rate which warms the lower troposphere and surface. The difference in temperature shown in the AGCM simulations is generally larger than the difference in heating rate shown in the off-line calculations. This is due to the positive feedback between the temperature and water vapor amount mentioned above.

In the top panels of Fig.7, the two seasonal (JJA and DJF) mean global distributions of the downward solar irradiances at the surface based on the simulations using the Thuillier spectrum are presented. It is seen that the downward solar irradiance is much larger in the northern hemisphere in the summer season and the opposite result happens in the southern hemisphere. In the lower panels (second to fourth rows), the differences in the downward solar irradiance are presented. It is seen that changes in solar spectra can cause changes in solar irradiance at the surface as large as 3 W m^{-2}, which is much lager than that due to the aerosol forcing (Nicolas et al., 2005). The difference is also larger in the summer hemisphere than in the winter hemisphere. Of the three model spectra, Kurucz10 has the largest difference in the downward irradiance and Kurucz95 has the smallest difference compared to that of the Thuillier spectrum. This is consistent with the off-line broad band results as shown in the upper left panel of Fig.5.

In Fig.8, the impacts on the surface temperature due to changing the solar spectra are presented. The upper two panels show the surface temperatures produced by the reference Thuillier spectrum, for the two seasons of JJA and DJF. The lower panels show the differences in surface temperature between the model spectra and the reference spectrum. The two Kurucz spectra produce lower surface temperatures compared to the Thuillier spectrum. It is seen that the temperature response to the changes in solar spectra is in a range of $\pm$2K. As seen in Fig.7, using the Kurucz10 spectrum leads to more solar irradiance (and hence, solar energy) reaching the surface. The surface temperature, however, does not respond in the same direction as this forcing. We therefore need to understand the related physical reasons behind this behavior. An obvious reason is that the surface albedo is very different in the different

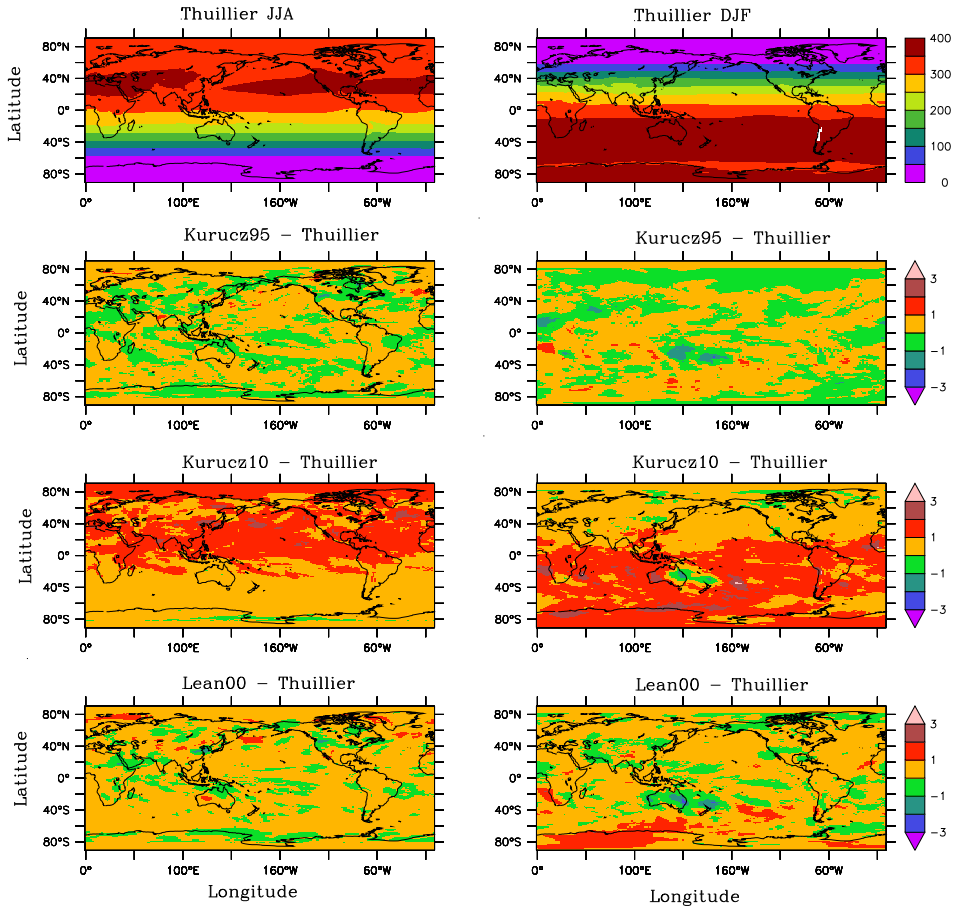

Fig. 7. Compared in the upper panel are the total downward solar irradiance (W m^{-2}) at the surface determined using the reference solar spectrum for winter (DJF) and summer (JJA) seasons with those determined by the model solar spectra, shown as separate differences (model minus reference) separately in the bottom three panels.

spectral regions. Generally, the surface albedo is relative lower in the NIR range and higher in the UV and VIS range. A higher surface albedo indicates a stronger surface reflection, which limits the energy absorption by the surface and produces a lower surface temperature. The surface albedo in the NIR is about 1/3 of that in the UV and VIS. Therefore, the surface solar energy absorption is largely determined by the downward solar radiation in the NIR range. In Fig.5, it has been shown that the Kurucz10 spectrum produces the lowest downward irradiance at the surface in the NIR range. This explains why the Kurucz10 spectrum produces the lowest surface temperature. Following the same argument, we can understand why the Lean00 spectrum produces the relatively highest surface temperature as shown in Fig.8, since the Lean spectrum corresponds to the largest downward solar irradiance in the NIR range.

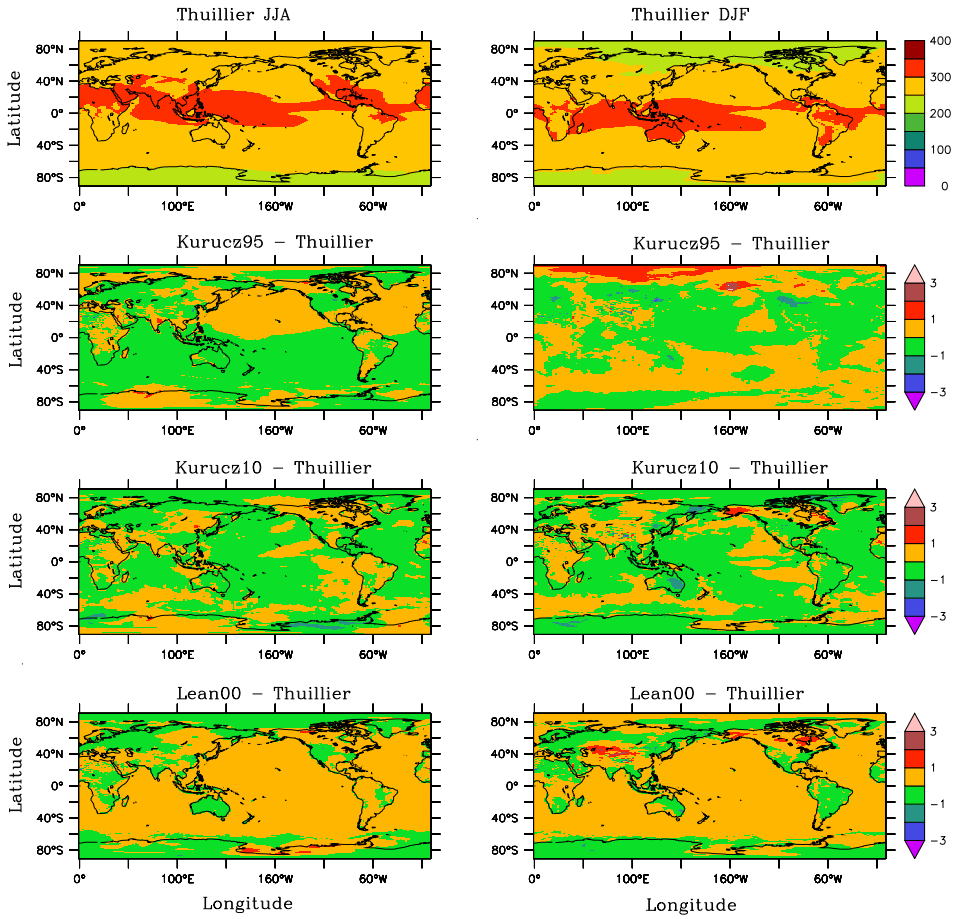

Fig. 8. Compared in the upper panels are the surface temperature distributions determined by the ACCESS model for two seasons using the reference solar spectrum with those determined using the model spectra displayed as separate differences in the bottom panels.

5. Summary and conclusions

In this chapter, we have analyzed the solar spectra currently used in climate models. The radiative impacts of the solar spectra are examined by using high spectral resolution line-by-line and broad-band radiative transfer models. It has been found that the solar heating rate in the stratosphere is very sensitive to the solar spectral distribution at the top of the atmosphere. The most sensitive spectral region is in the Hartley band near 300 nm where ozone has a strong absorption. The solar energy fraction from the Kurucz95 spectrum in this region is relative larger and the use of this spectrum leads to a large solar heating in the upper stratosphere. The modified spectrum of Kurucz10 contains an even larger proportion of energy in this region, which produces an even higher heating rate. The Lean00 spectrum which includes the latest observations from space platforms produces heating rates close to those using the reference Thuillier spectrum.

It is found that the radiative impact of the solar spectra is not limited to the ozone absorption in the UV range. The water vapor absorption in the lower atmosphere and the downward solar irradiance at the surface are also strongly influenced by the choice of the solar spectra. The effects of changes in the solar spectral distribution on the solar irradiance in three major spectral regions are much larger than on the total irradiance. The maximum difference in the total irradiance among the five solar spectra is about 2 W m^{-2} whereas those in the three spectral band irradiances are about 6 - 9 W m^{-2}. These spectral differences will in turn influence important processes, such as the forecast UVB, land-surface processes, and sensible and latent heat fluxes.

Four solar spectra have been evaluated using the ACCESS climate model. The climate model simulations show that the temperatures in the stratosphere and above from the Kurucz95 and Kurucz10 spectra are systematically higher than the result using the Thuillier spectrum. The difference is up to 5 K. On the other hand the stratospheric temperature due to use of the Lean00 spectrum is generally lower than the result using the Thuillier spectrum. In the lower atmosphere the Lean00 spectrum produces a noticeable warming bias compared to that of the Kurucz spectrum because this data contains a larger portion of incoming solar energy in the NIR range.

The climate model simulations also show that the changes in solar spectra can influence the downward solar irradiance at the surface. The difference can be as large as 3 W m^{-2} for different solar spectra. The changes in the downward solar irradiance is expected to have an influence on the surface temperature. However, it is interestingly found that the larger downward total solar irradiance at the surface does not necessarily correspond to higher surface temperature. The surface temperature strongly relies on the surface albedo and the surface albedo is generally much lower in the NIR range. Therefore the surface solar energy absorption is largely determined by the downward solar radiation in the NIR range.

From the results presented in this study, we cannot make a recommendation on which solar spectra should be used in a climate model because of the lack of the necessary comparison with observations. However, our results are of use for future work. For example, it may be better to examine the solar spectra against observations in the UV spectral region. This is because the differences in the solar irradiance amongst the five spectra are largest in this region where only the ozone absorption is important. The calculations in this region are not influenced by uncertainties from water vapour and other absorbing species. Although we cannot make a general recommendation our results suggest that the Lean00 spectrum should be used in the ACCESS (UM) model as it can reduce the model warm bias as identified by Zhong *et al.* and the current study.

6. Acknowledgment

Kurucz10 spectrum were downloaded from http://www.cfa.harvard.edu/atmosphere.

Prof. Gerard Thuillier is thanked for providing the solar spectrum used as a reference in this study.

Dr. Jingmiao Liu is supported by the Chinese National Natural Science Foundation of the project management under the grant No. 40775020

Dr. Lawrie Rikus is thanked for reviewing the manuscript.

7. References

Chance, K. & Kurucz, R. L. (2010). An improved high-resolution solar reference spectrum for earth's atmosphere measurements in the ultraviolet, visible, and near infrared, *J. Quant. Spec. Rad. Tran.*, Vol. 111, No. 9, (June 2010), pp.(1289-1295), 0022-4073.

Davies, T.; Cullen, M.J.P.; Malcolm, A.J.; Mawson, M.H. & Staniforth, A. (2005). A new dynamical core for the Met Office global and regional modelling of the atmosphere, *Q. J. R. Meteorol. Soc.*, Vol. 131, No. 608, (April 2005), pp. (1759-1782), 0035-9009.

Edwards, D.P. (1992). GENLN2: A general line-by-line atmospheric transmittance and radiance model, *Technical Note TN-367+STR*, NCAR: Boulder, Colorado, USA.

Gao, B.-C. & Green, R. (1995). Presence of terrestrial atmospheric gas absorption bands in standard extraterrestrial solar irradiance curves in the near-infrared spectral region, *App. Opt.*, Vol. 34, No. 27,(September 1995), pp. (6263-6268), 1559-128X.

Kopp, G & Lean, J. L. (2011). A new, lower value of total solar irradiance: Evidence and climate significant, *Geophys. Res. Lett.*, Vol. 38, No. L01706, (January 2011),pp. 7, 0094-8276.

Kurucz, R. L. (1995). The solar irradiance by computation, In: *Proceedings of the 17th Annual Conference on atmospheric transmission models*, Anderson, G. P.; Picard, R. H. & Chetwind, J. H. (ed.), 205-258, Phillips Laboratory Directorate of Geo-physics, PL-TR-95-2060, Hanscom Air Force Base, Mass.

Lean, J. (2000). Evolution of the Sun's spectral irradiance since the Maunder Minimum, *Geophys. Res. Lett.*, Vol. 27, No. 16, (August 2000), pp. (2425-2428), 0094-8276.

Mlawer, E.J.; Brown, P.D.; Clough, S.A.; Harrison, L.C.; Michalsky, J.J.; Kiedron, P.W. & Shippert, T. (2000). Comparison of spectral direct and diffuse solar irradiance measurements and calculations for cloud-free conditions, *Geophys. Res. Lett.*, Vol. 27, No. 17, (September 2000), pp. (2653-2656), 0094-8276.

Neckel, H. & Labs, D. (1984). The solar radiation between 3300 and 12500 Å, *Solar Physsics*, Vol. 90R, No. 2, (February 1984), pp. (205-258), 0038-0938.

Krivova, N. A.; Vieira, L. E. A. & Solanki, S. K. (2010). Reconstruction of solar spectral irradiance since the Maunder minimum, *J. Geophys. Res.*, Vol. 115, No. A12112, (December 2010), pp.(11), 0148-0227.

Nicolas, B.; Boucher, O.; Haywood, J. & Reddy, M.S. (2005). Global estimate of aerosol direct radiative forcing from satellite measurements, *Nature*, Vol. 438, No. 22, (December 2005), pp. 1138-1141, 0028-0836.

Stokes G. M & Schwartz S. E. (1994). The Atmospheric Radiation Measurement (ARM) Program: Programmatic background and design of the cloud and Radiation Testbed, *Bull. Amer. Meteor. Soc*. Vol. 75, No. 7, (July 1994), pp. 1201-1221, 0003-0007.

Sun, Z. (2011). Improving transmission calculations for Edwards-Slingo radiation scheme using a correlated k-distribution method, *Q. J. R. Meteorol. Soc.*, In press.

Thuillier, G.; Herse, M.; Labs, D.; Foujols, T.; Peetermans, W.; Gillotay, D.; Simon, P. C. & Mandel, H. (2003). The solar spectral irradiance from 200 to 2400 nm as measured by the SOLSPEC spectrometer from the ATLAS and EURECA missions. *Solar Physics*, Vol. 214, No. 1, (May 2003), pp. 1-22, 0038-0938.

Zhong, W.; Osprey, S.M. & Haigh, J.D. (2008). Influence of the prescribed solar spectrum on calculations of atmospheric temperature, *Geophys. Res. Lett.*, Vol. 35, No. L22813, (November 2008), pp. 5, 0094-8276.

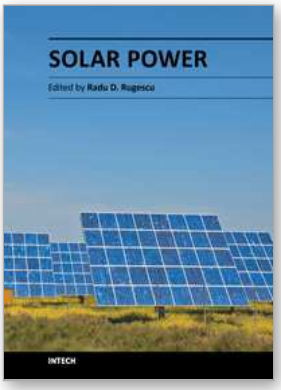

Solar Power

Edited by Prof. Radu Rugescu

ISBN 978-953-51-0014-0
Hard cover, 378 pages
Publisher InTech
Published online 15, February, 2012
Published in print edition February, 2012

A wide variety of detail regarding genuine and proprietary research from distinguished authors is presented, ranging from new means of evaluation of the local solar irradiance to the manufacturing technology of photovoltaic cells. Also included is the topic of biotechnology based on solar energy and electricity generation onboard space vehicles in an optimised manner with possible transfer to the Earth. The graphical material supports the presentation, transforming the reading into a pleasant and instructive labor for any interested specialist or student.

InTech Europe
University Campus STeP Ri
Slavka Krautzeka 83/A
51000 Rijeka, Croatia
Phone: +385 (51) 770 447
Fax: +385 (51) 686 166
www.intechopen.com

InTech China
Unit 405, Office Block, Hotel Equatorial Shanghai
No.65, Yan An Road (West), Shanghai, 200040, China
中国上海市延安西路65号上海国际贵都大饭店办公楼405单元
Phone: +86-21-62489820
Fax: +86-21-62489821